NUMERICAL STUDY OF THE IMPACT OF AN ALUMINA DROPLET IN THE PLASMA SPRAYING PROCESS

Mouloud DRIOUCHE[1, *], Tahar REZOUG[2], Mohammed EL GANAOUI [2]

In this paper, a CFD based numerical model has been developed that can describe the impact of an alumina droplet on a stainless-steel substrate. In this model, the equations of this multiphysics problem, including fluid dynamics, multiphase flow, and heat transfer with solidification, are solved by the finite volume method using Ansys Fluent 16 software. Following the validation of the model through a comparison of its results with those obtained through experimentation published, it was employed to investigate the impact velocity-dependent in splat morphology and solidification. It was observed that the splat obtained is unfragmented disk-shaped, has a larger diameter and solidifies faster at higher impact velocities, which favors good adhesion between the splat and the substrate. A new relationship between Reynolds number and maximum spreading factor was established with these results.

Keywords: Alumina droplet, Impact, Solidification, Plasma spray, CFD.

1. Introduction

The phenomenon of droplet impact on solid surfaces occurs in many industrial applications such as thermal spray coating, cooling of hot surfaces, in-flight icing, and inkjet printing. Several thermal spraying techniques are used in the manufacture of functional coatings. The coatings in question have mechanical, physical and biological properties that make them very useful in today's functional coating applications [1]. In the industrial context, the cooling of hot surfaces is an unavoidable imperative, as is nuclear safety. Cooling processes are mainly based on the impact of liquid jets or sprays, where droplets play a crucial role. The optimum efficiency of spray cooling is due to the prolonged cooling time of the liquid jet and the high consumption of the liquid [2]. Accretion, resulting from the impact freezing of supercooled droplets, has a significant impact on the aerodynamics of aircraft wings, which can compromise flight safety. In recent

* Corresponding author
[1] PhD, Blida1 University, Institute of Aeronautics and Space Studies, Laboratory of Aeronautical Sciences, Algeria, e-mail: driouche_mouloud@univ-blida.dz
[2] Prof, Blida1 University, Institute of Aeronautics and Space Studies, Laboratory of Aeronautical Sciences, Algeria, e-mail: trezoug@yahoo.fr
[3] Prof, University of Lorraine, LERMAB, IUT H Poincaré de Longwy, France, e-mail: mohammed.el-ganaoui@univ-lorraine.fr

times, superhydrophobic surfaces have attracted growing interest because of their remarkable anti-icing properties [3]. As part of the study carried out on printing processes, it was established that the quality and cost of printing with various inks, whether for traditional applications, ceramic-based 3D printing, 3D printing of organs or printing for electronic applications, depend on control of the size of the micro droplets [4]. Plasma thermal spraying is a process used in a wide range of industries including aerospace, mechanical engineering, marine and medical. The resulting coatings protect parts from wear, corrosion, oxidation and high temperatures [5-6]. In aeronautics, plasma thermal spraying is used to create thermal barrier coatings (TBC) to protect jet engine blades from high temperatures, thereby improving propulsion efficiency [7-8]. The coating consists of a stack of particles that are propelled by the plasma jet and subjected to extremely high temperatures. Consequently, the particles are either wholly or partially molten and impact the substrate at varying speeds contingent on their trajectory within the jet. The quality of the coating is contingent upon the adhesion strength, which is defined by the first droplets to spread out on the substrate [1, 9].

Much research has been done to understand the multiphysics involved in deposit formation by studying the impact, spreading, and solidification of individual droplets. Their spreading and solidification take only a few micron seconds, making experimental expertise very difficult [10]. However, most research has focused on numerical modelling. Alavi et al [11] proposed a numerical method to study the impact of a molten and semi-molten nickel particle. To simulate the motion of solid cores, they assigned a significant viscosity to this region. Their results show that the size of the solid core affects how splashing of semi-molten particles occurs. In a study by Oukach et al. [12], a correlation was identified between the spreading factor and the Reynolds number, using the finite element method to simulate the impact of a molten ceramic droplet. In their study, the droplet/air interface is captured using the level set method. Shen et al. [13] employed numerical techniques to solve the coupled Navier-Stokes and Cahn-Hilliard equations. The introduction of latent heat as a source term in the energy equation enabled the solidification front to be tracked. They positively confirmed their results with those obtained experimentally. Le Bot et al [14] proposed a numerical model to describe the effect of several successive droplets. They found that the interaction of droplets with the substrate or with neighboring droplets induces variable porosity in the coating. Driouche et al. [15] conducted a numerical investigation into the impact of the size of ceramic droplets impacting the substrate on their spreading and solidification, as well as on the melting of the substrate. The model has been validated by comparing these results with published experimental results. Patel et al [16] investigated the influence of plasma projection parameters on the impact of dense and hollow

molten droplets. In their study, a FORTRAN95 code was employed for the solution of the equations using the finite volume method. The findings were found to be in accordance with the results of previous experiments.

The maximum spreading factor (ξ) is defined as the ratio between the diameter of the spreading droplet and its initial diameter. It is a crucial parameter for quantifying the quality of a coating. In the context of thermal spraying, the maximum spreading factor is contingent upon the Reynolds number (Re) [9]. Several attempts have been made to determine a simple expression for the spreading factor. Madjeski [17] developed a theoretical model using the one-dimensional Stefan approach to solidification and two-dimensional radial flow. Viscous, inertial and surface tension effects were considered. He is among the first to derive a spreading factor relation ($\xi_{\max} = 1.294 R_e^{0.2}$). Shinoda et al [18] experimentally studied the impact of zirconia droplets at velocities between 10 and 70 m/s. They derived a maximum degree of spreading relationship ($\xi_{\max} = 0.43 R_e^{1/3}$) to predict the final droplet morphology. Bertagnoli et al. [19] established a correlation between the spreading factor ($\xi_{\max} = 0.925 R_e^{0.2}$) derived from a finite element method-based model and the physical phenomena involved in the impact process of a ceramic droplet. In their study, Zhang et al. [20] employed numerical simulation to investigate the impact of temperature, velocity, and contact angle on the behaviour of a plasma-sprayed nickel droplet, and proposed a relationship for the maximum spreading factor ($\xi_{\max} = 1.208 R_e^{0.128}$).

The objective of this study is to develop a numerical model for simulating the impact of an alumina (Al_2O_3) droplet on a stainless-steel substrate under plasma spray conditions. The proposed model is based on the solution of the equations of dynamics combined with the Volume of Fluid (VOF) method, which is employed to capture the free surface of the droplet. Heat transfer and liquid/solid phase change are considered by solving the energy equation and using the enthalpy porosity technique to track the solidification front. The equations are discretized in a 2D axisymmetric domain by the finite volume method, utilizing the ANSYS FLUENT 16.0 software [21]. Validation of the model is achieved through a comparison of the results obtained for the impact case of a millimeter tin droplet with the experimental results existing in literature. The influence of the impact velocity on the splat morphology was also investigated. A new correlation is finally derived from the results to predict the maximum spreading factor.

2. Numerical model

The vertically impact of a spherical molten alumina droplet with a diameter of 40 μm at 2800 K on a stainless-steel stationary substrate preheated to 450 K is examined. Transient flow and heat transfer with solidification are

modelled in a 2D axisymmetric domain, as shown in Fig 1. The droplet impact velocity is varied from 50 m/s to 200 m/s to study its effect on the splat formation. In developing the model, the following assumptions were taken into account :

a. The flow of the droplet and the surrounding air was incompressible, laminar and Newtonian
b. Contact thermal resistance and surface tension were kept constant.
c. The physical properties of the droplet, surrounding air and substrate were constant.
d. Heat transfer is dominated by convection and conduction, ignoring radiation.

2.1. Fluid dynamics

The Navier-Stockes equations are discretized by the finite volume method. These equations can be expressed:

$$\nabla \cdot \vec{v} = 0 \tag{1}$$

$$\frac{\partial(\rho\vec{v})}{\partial t} + \nabla \cdot (\rho\vec{v}\vec{v}) = -\nabla P + \nabla \cdot [\mu(\nabla\vec{v} + \nabla\vec{v}^{\tau})] + \rho\vec{g} + F_{vol} + S_y \tag{2}$$

Where $\vec{v}$ is the velocity vector, P is the pressure, $\vec{g}$ is the gravity vector, F_{vol} is the surface tension force per unit volume, $\mu(\nabla\vec{v} + \nabla\vec{v}^{\tau})$ is the viscosity stress tensor, S_y is the source term, ρ is the density, and μ is the dynamic viscosity. The VOF method is employed to capture the free surface of the droplet. A scalar function, designated as α_l, is utilised to represent the volume fraction of the liquid (droplet) within a given cell. When the liquid occupies a cell, α_l is assigned a value of 1, whereas when it is absent, α_l is set to 0. At the interface between the droplet and the surrounding air, α_l assumes a value between 0 and 1. The free surface of the droplet is tracked by solving the following equation:

$$\frac{\partial\alpha_l}{\partial t} + \vec{v} \cdot \nabla\alpha_l = 0 \tag{3}$$

This equation will not be solved for the volume fraction of air, noted α_g, it will be calculated by the following equation:

$$\alpha_g + \alpha_l = 1 \tag{4}$$

The source term F_{vol} in equation (2) is a volume force that models the surface tension. This force is determined using the continuous surface force (CSF)

technique [22]. This technique is also employed to forecast the curvature of the droplet surface in the vicinity of the substrate wall. The contact angle of the droplet with the substrate is maintained at a constant value of 90°.

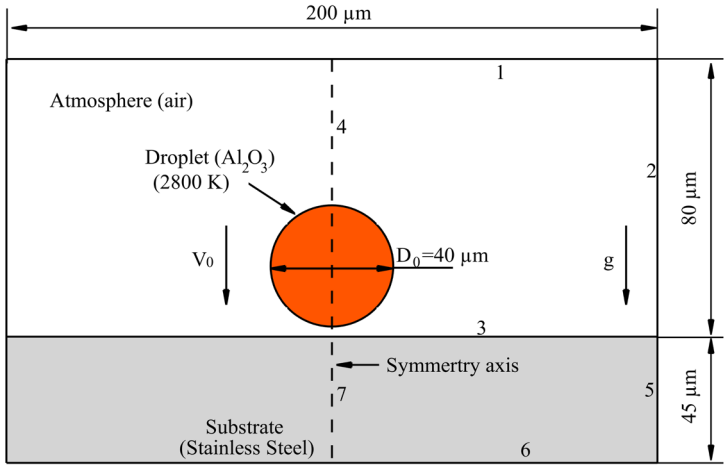

Fig. 1. 2D axisymmetric domain for droplet impact simulation, labels : 1 to 7 refer to boundaries.

2.2. Heat Transfer and solidification

The enthalpy porosity technique [23] is adopted to model droplet solidification. The liquid fraction (f_l) is a quantity assigned to each cell, indicating the liquid state of the fluid. To determine the liquid fraction, an enthalpy balance is employed.

A value of zero for f_l indicates the presence of solid material in the cell, while a value of one for f_l indicates the presence of only liquid. Between these two values, a pasty zone is defined. The liquid fraction is defined by the following equation:

$$\begin{aligned} f_l &= 0 && \text{if } T < T_{solidus} \\ f_l &= \frac{T - T_{solidus}}{T_{liquidus} - T_{solidus}} && \text{if } T_{solidus} < T < T_{liquidus} \\ f_l &= 1 && \text{if } T > T_{liquidus} \end{aligned} \tag{5}$$

The total enthalpy is defined as the sum of the sensible and latent heat, as follows:

$$H = h + \Delta H, h = h_{ref} + \int_{T_{ref}}^{T} C_P dT \tag{6}$$

In this context, h_{ref} and T_{ref} represent the sensible enthalpy and reference temperature, respectively, while C_P denotes the specific heat at constant pressure.

It is important to note that the latent enthalpy is a function of temperature. In the mushy zone, the latent heat of fusion, denoted by ΔH, can be expressed as a fraction of the latent heat of fusion L.

$$\Delta H = f_l L \tag{7}$$

In conclusion, the energy equation for droplet solidification can be expressed as follows:

$$\frac{\partial}{\partial T}(\rho H) + \nabla \cdot (\rho \vec{v} H) = \nabla \cdot (k \nabla T) + S_h \tag{8}$$

Where k is the thermal conductivity and S_h is a source term defined as follows:

$$S_h = \frac{\partial}{\partial t}(\rho \Delta H) + \nabla(\rho v \Delta H) \tag{9}$$

The Darcy source is employed for the purpose of defining the motion within the mushy zone. When f_l is close to zero during solidification, the flow velocity tends to zero. This approach is predicated on the modification of equation (2) through the utilisation of the S_y source term.

$$S_y = \frac{(1-f_l)^2}{(f_l^3 + \varepsilon)} A_{mush} v \tag{10}$$

The value of ε is taken to be a small number (0.001) in order to avoid uncertainty. The constant A_{mush} represents the slope of the velocity drop towards zero as the material solidifies. The value of A_{mush} is set to 10^9 [24]. To account for imperfect contact at the droplet/substrate interface, a contact thermal resistance of $10^{-7}\, m^2 K / W$ is considered.

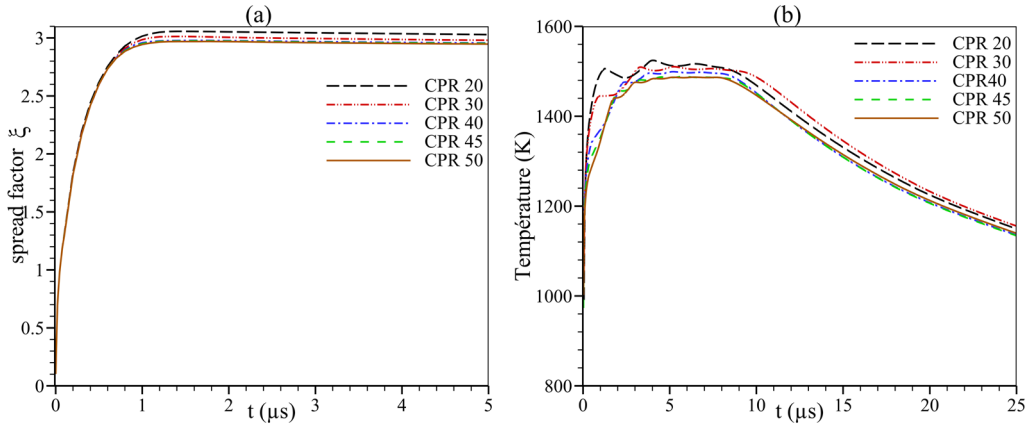

Fig. 2. A mesh test on the spreading factor (a), and temperature history at the centre of the substrate surface (b). The case study of the impact of a 40 µm diameter alumina droplet at 2800 K, at 100 m/s, on a stainless-steel substrate at 450 K.

2.3. Discretization methods

As shown in Figure 1, the dimensions of the domain are represented, while the boundary conditions are summarised in table 1. The thermophysical properties of the droplet and substrate are presented in table 2. A structured mesh was chosen for the simulations, and a parameter called CPR (Cell Per Radius) was adopted to size the meshes. Mesh refinement was conducted in the vicinity of the droplet/substrate interface, where heat exchange is of particular significance. The QUICK scheme was employed to solve the energy and dynamics equations. The Compressive Interface Capturing Scheme for Arbitrary Meshes (CICSAM) was utilised to discretise the volume of fluid (VOF) equation. The CICSAM scheme is recommended for multiphase flows, where the viscosity ratio is very high (greater than 10^3), as in this problem. Pressure and velocity are coupled using the PISO technique. The PRESTO! scheme is deployed for pressure interpolation. A constant time step of 10^{-10} seconds is chosen for an implicit first-order formulation.

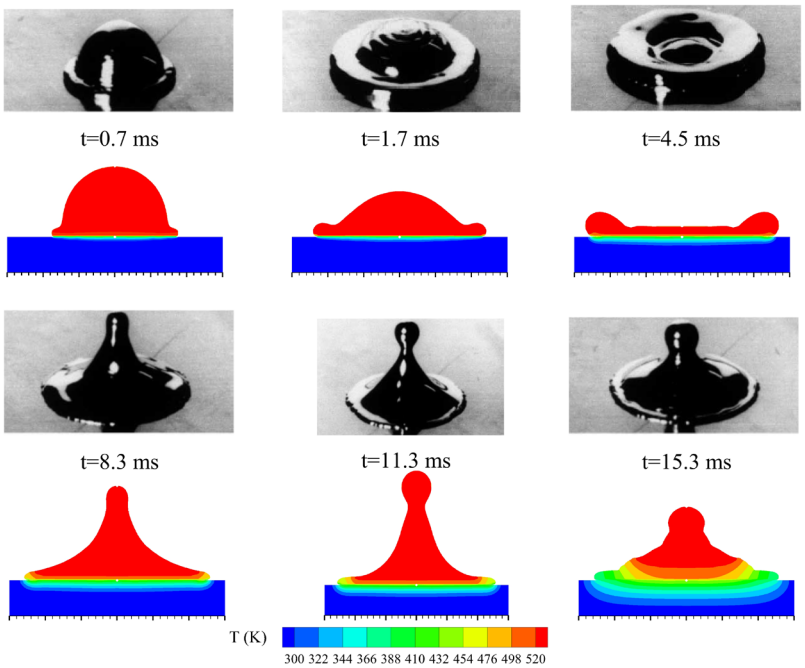

(a) Morphology

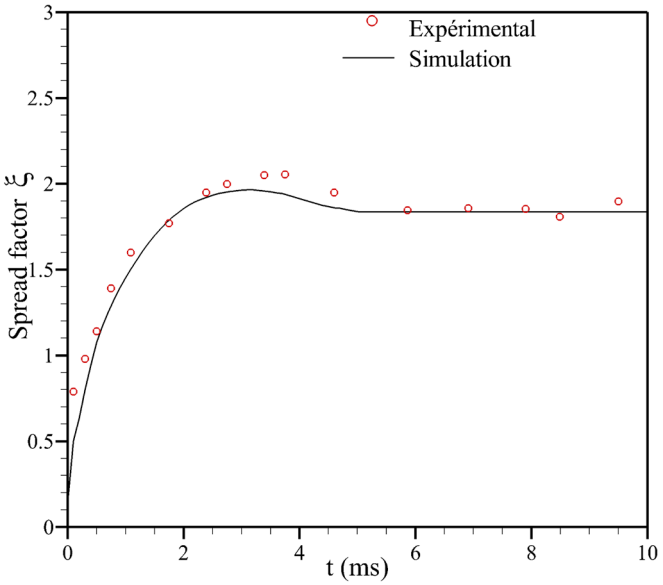

(b) Spread factor

Fig. 3. Comparison of simulation and experiment [25], for the case of impact of a 2.7 mm diameter tin droplet at 513K, with a velocity of 1 m/s on a stainless-steel substrate.

Table 1

Boundary conditions

Boundary	Navier-Stokes equations	Heat transfer equations
1, 2	Pressure outlet	Kept at 300 K
3	Wall-No slip	Wall-Contact resistance $10^{-7} m^2 K/W$
4	Axis	Axis
5,6	Not active	Wall kept at 300 K
7	Not active	Axis

2.2. Model validation

Simulations were performed on meshes of different sizes to test for mesh independence. Fig 2 illustrates the temporal evolution of the spreading factor and substrate surface temperature for distinct CPR values. The spreading factor and substrate surface temperature for CPR 40, 45, and 50 are practically identical. Therefore, a mesh corresponding to CPR 40 is used for all simulations.

In order to validate this model, a comparison was made between the simulation results and those obtained experimentally by Aziz et al. [25] for the case of a tin droplet impact.

Table 2

Thermophysical properties of the droplet and substrate

Properties	Alumina (Al2O3)	Stainless Steel
Density (kg/m^3)	3990	7930
Thermal conductivity (W/m K) (sol)	5.9	16.3
Thermal conductivity (W/m K) (liq)	7.86	-
Specific heat (J/kg K) (sol)	1273	540
Specific heat (J/kg K) (liq)	1358	-
Kinematic viscosity (m^2/s)	1.026x10^{-5}	-
Surface tension (N/m)	0.69	-
Melting Point (K)	2327	1673
Latent heat of fusion (J/kg)	1.16x10^6	-

The simulation was conducted with a velocity of 1 m/s at impact, a 2.7 mm in diameter at 513 K, on a stainless-steel substrate at 300 K. As illustrated in Fig 3a, following the impact event, the droplet undergoes a process of spreading and flattening on the substrate, reaching a state of equilibrium at t=4.5 ms, when it reaches its maximum spreading. The lower part solidifies, while surface tension forces the upper part, still in liquid state, to move backwards.

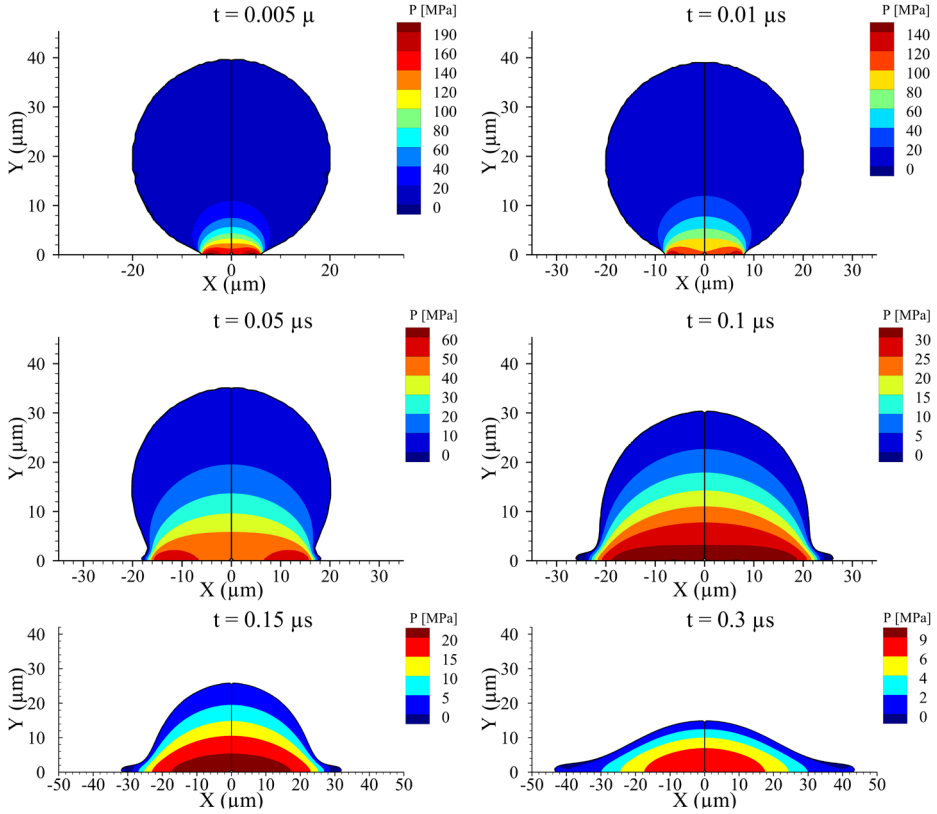

Fig. 4. The pressure fields during the impact of a 40 µm diameter alumina droplet at 2800 K with a velocity of 100 m/s on a stainless-steel substrate at 450 K.

The simulation accurately predicted the throttling of the upper part at t=11.3 ms. These results show good agreement between simulation and experiment. A comparison was also made using quantitative data in order to evaluate the uncertainties in the numerical results. As part of this study, a comparison was made between the spread factor obtained by the simulation and that measured [25]. The spread factor, both measured and simulated, are illustrated in Fig 3b. It is essential to note that the agreement with experiment is excellent, since the model predict a final spread factor of 1.83, while obtained experimentally reach 1.9, corresponding to an error of 3.68%.

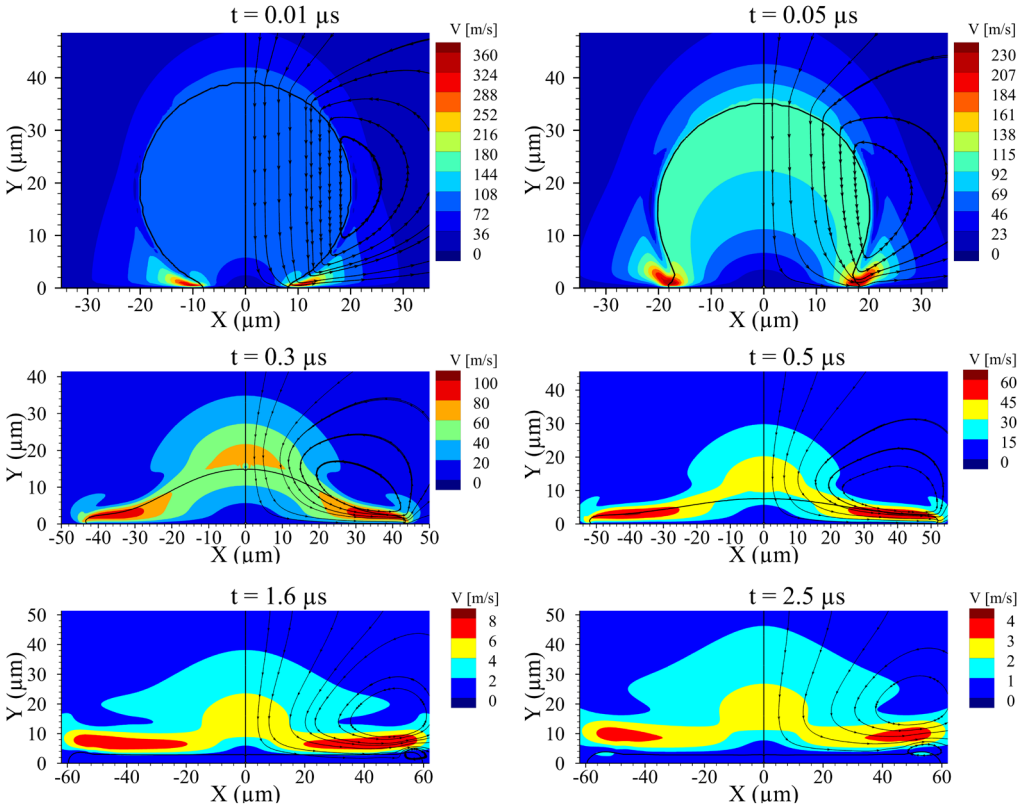

Fig. 5. The velocity fields and current lines in the droplet and in the air during the spreading of a 40 µm diameter alumina droplet at 2800 K with a velocity of 100 m/s on the stainless-steel substrate at 450 K.

3. Results and discussion:

Fig 4 illustrates the evolution of pressure as the droplet contacts and spreads across the substrate. Upon impact, the droplet's velocity diminishes significantly, resulting in a conversion of kinetic energy to potential energy. This phenomenon leads to an increase in pressure at the droplet/substrate interface. The

pressure at the contact point reaches a markedly elevated value (approximately 190 MPa) in a remarkably brief interval (0.005 μs). Because of the considerable pressure within the droplet, the latter undergoes deformation and radial expansion. As this happens, the pressure decreases rapidly and reaches about 60 MPa at t=0.05 μs. The pressure maximum shifts from the centre to the edge of the droplet, and this pressure wave propagates through the droplet without reaching the entire droplet. In the radial direction, the pressure becomes uniform, but it remains relatively high in the vicinity of the substrate.

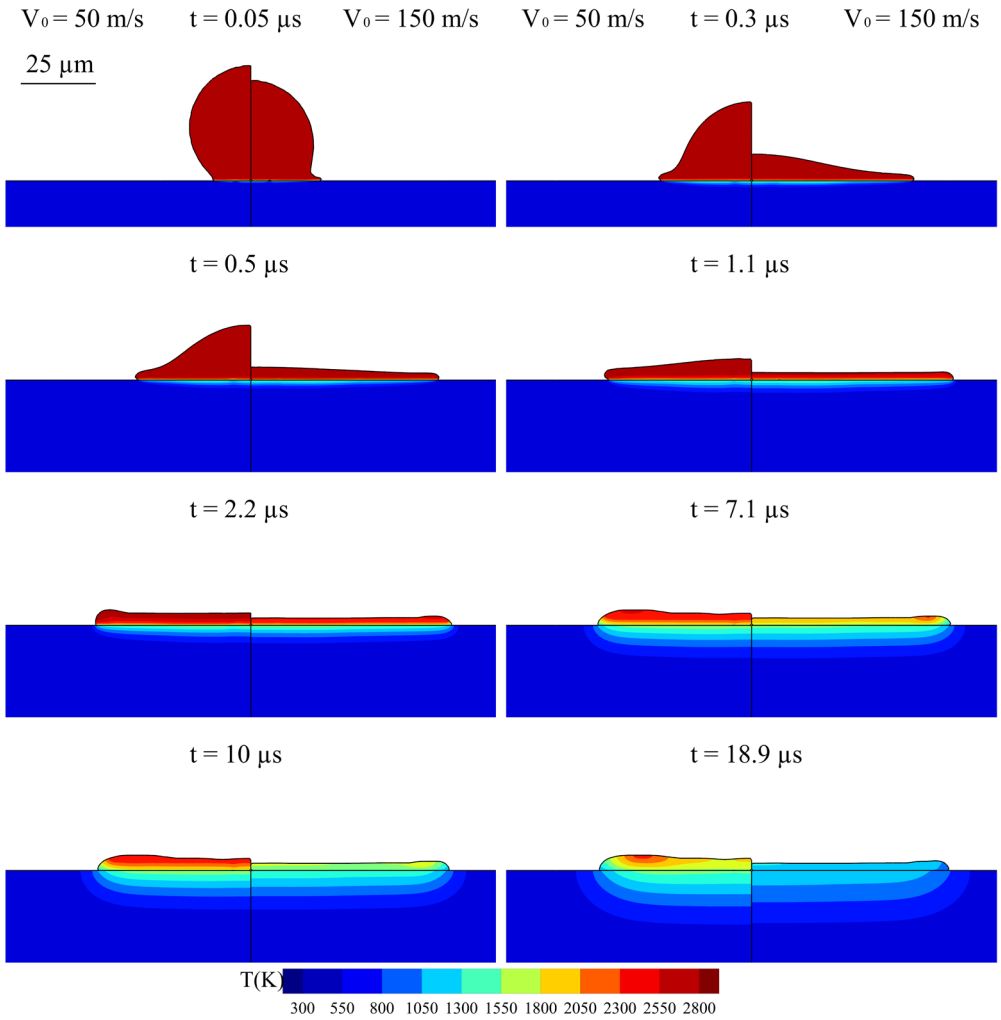

Fig. 6. The spreading and temperature distribution of the droplet and substrate. The images on the right for 150 m/s, on the left for 50 m/s.

The pressure increase that occurs immediately following the impact causes the fluid that is flowing along the substrate to accelerate to a high velocity in the

radial direction, which is represented in Fig 5. At 0.01 µs, the flow velocity in the centre of the droplet decreases rapidly as a result of the influence of the wall. Conversely, at the outer ends of the droplet, the velocity increases to 360 m/s, which is more than three times the initial impact velocity (100 m/s). This value is in close alignment with that reported by Li et al. [26]. The velocity in the upper part of the droplet is practically equal to the initial impact velocity. As the droplet spreads, it causes the initially stationary air to move, forming two primary vortices above the substrate, i.e., the air is driven out by the droplet. The flow velocity declines in a gradual manner over time, reaching a value of 60 m/s at t=0.5 µs. The maximum velocity is consistently observed at the outer extremities of the droplet.

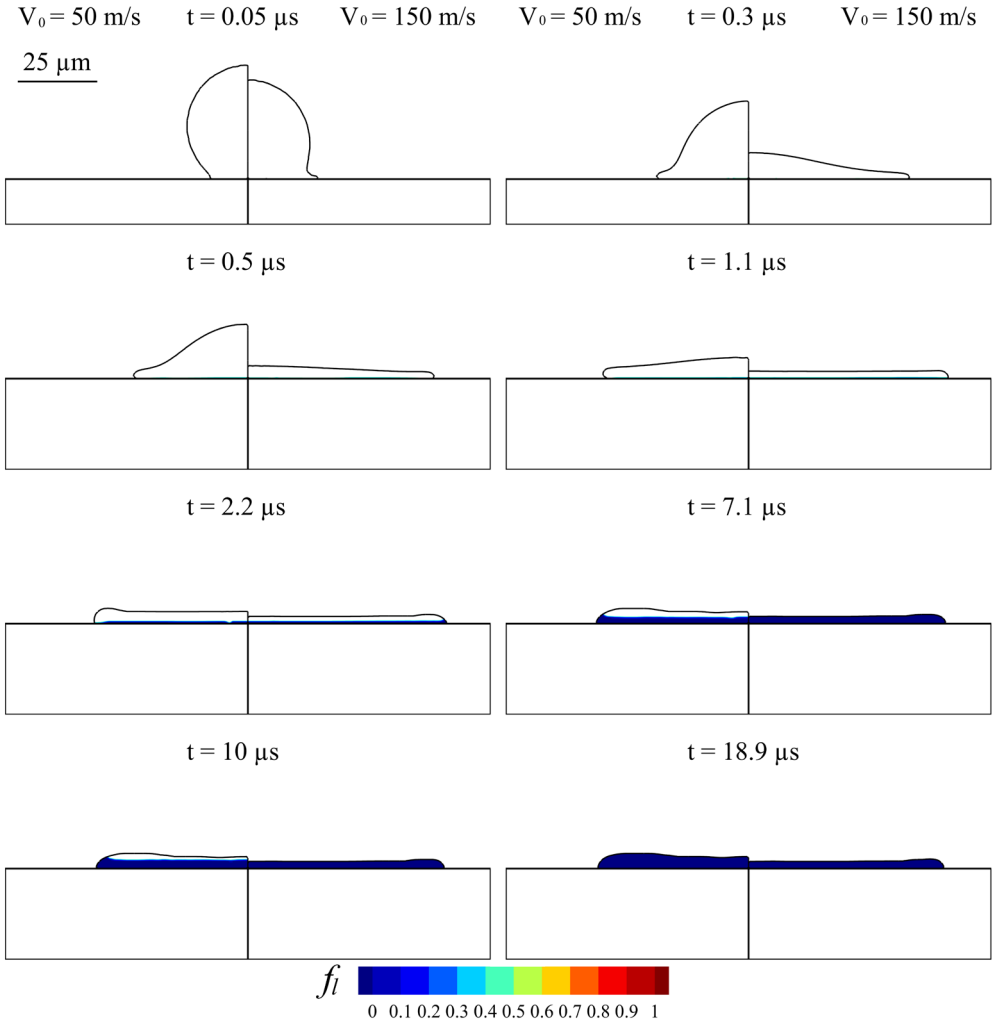

Fig. 7. progress of solidification of the alumina droplet. Impact velocity is 150 m/s (right-hand side of each image), and 50 m/s (left-hand side of each image).

Complete spreading of the droplet is attained at 1.6 µs, at which point the velocity within the droplet is markedly reduced, resulting in an almost negligible force of inertia. At this juncture, the surface tension exerts a slight recoil force on the upper portion of the droplet at tip, thereby creating a new recirculation zone that is counter to the primary vortex.

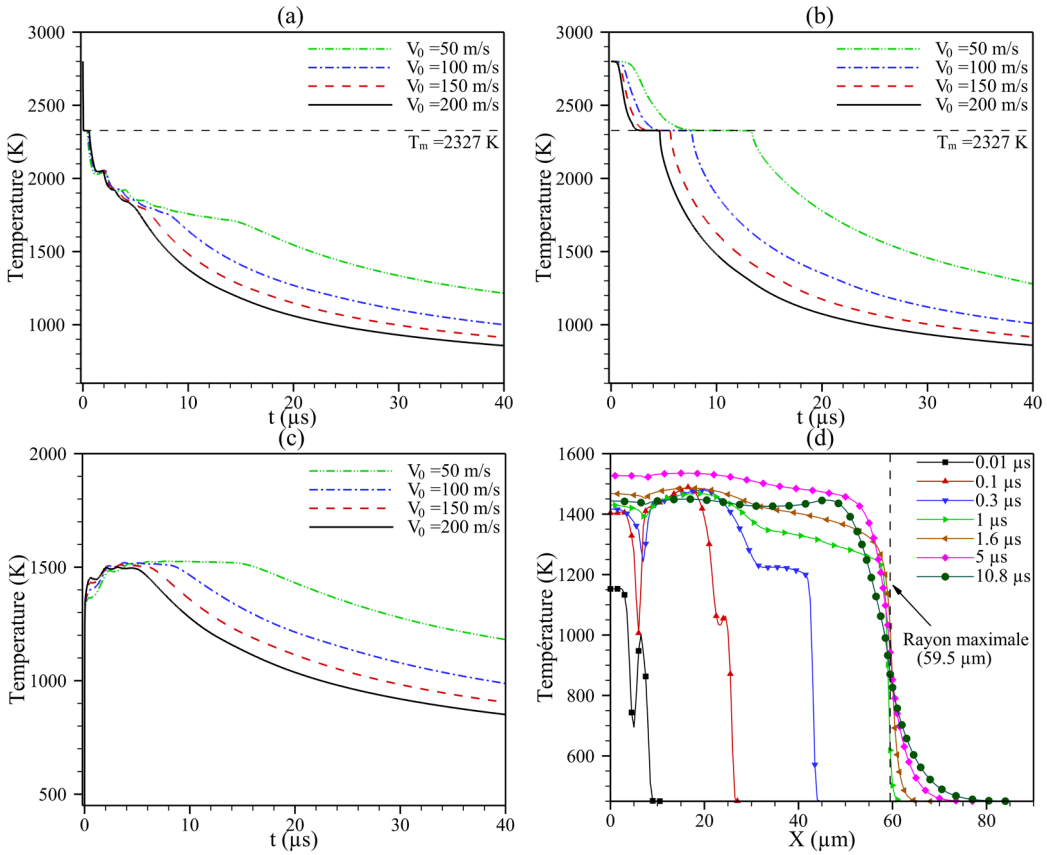

Fig. 8. The temperature history at the centre of the splat's bottom surface (a), splat's top surface (b), and the substrate surface (c) for different impact velocities. The temperature along the substrate surface for an impact at 100 m/s.

Fig 6 illustrates the spreading and time distribution of temperature in the droplet and substrate, for two impact velocities: 50 m/s (left side) and 150 m/s (right side). In both cases, the droplet spreads radially immediately after impact. It is very clear that the droplet with 150 m/s at impact spreads more rapidly, reaching its maximum at 1.1 µs versus 2.2 µs for the second droplet, which is almost twice the time. The recoil phenomenon is more pronounced at low impact velocities, because the dissipation of kinetic energy occurs earlier. The substantial temperature disparity between the droplet and the substrate gives rise to a considerable transfer of energy. The droplet, initially at 150 m/s upon impact,

undergoes a rapid cooling process. At the conclusion of its spreading, the substrate exhibits a greater heating in the radial direction than in the depth, in comparison to the 50 m/s droplet at impact. Finally, the final splat is disk-shaped, with slightly rounded edges.

The solidification of the droplet is illustrated in Fig 7. Because of the rapid cooling of the lower surface of the droplet, the solidification of this part commences immediately following the impact. At 0.3 µs, a thin solid layer is observed. Due to the rapid spreading and flattening of the droplet impacting at 150 m/s, solidification proceeds rapidly, and the droplet is completely solidified at t=7.1 µs, at which time the droplet impacting at 50 m/s is half solidified. It reaches full solidification at 18.9 µs, which is more than twice the solidification time of the droplet impacting at 150 m/s.

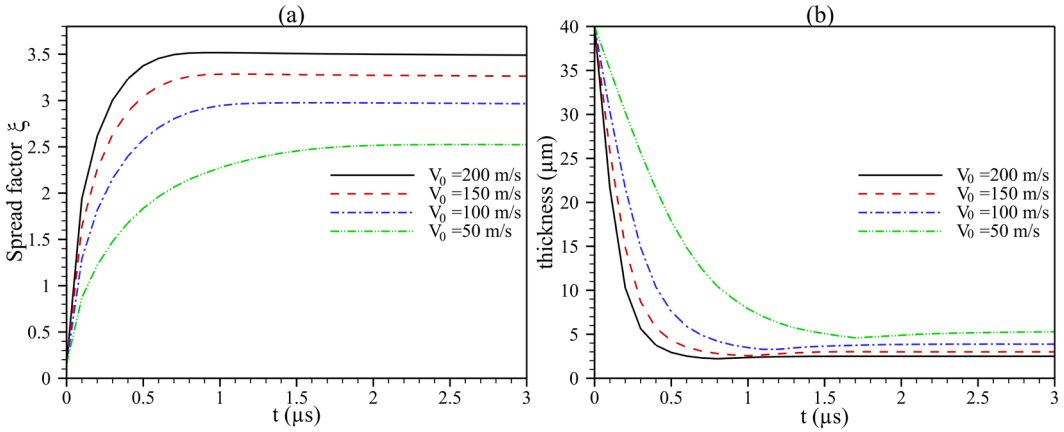

Fig. 9. Time evolution of spreading factor (a) and droplet thickness (b) for different impact velocities.

Fig 8a illustrates the temperature history of the bottom of the droplet. The cooling occurs rapidly for varying impact velocities, with the temperature dropping below the melting point (2327 K) and this portion beginning to solidify concurrently (t=0.16 µs). Nevertheless, the rate of cooling beyond solidification is contingent upon the impact velocity, with higher velocities resulting in accelerated cooling. This same tendency towards the top of the droplet is evident in Fig 8b. However, the temperature drops below the melting point takes a little longer, which is inversely proportional to the impact velocity: 12.37 µs, 7.08 µs, 5.12 µs, and 4.42 µs, respectively, for velocities of 50 m/s, 100 m/s, 150 m/s and 200 m/s. After solidification, cooling is faster at higher velocities, which is favorable for a lamellar structure because the droplets immediately impact the solidified spalt, are not splashed. A similar pattern is evident in Fig 8c, which depicts the heating and cooling of the substrate surface. The droplet with an impact velocity of 50 m/s exhibits a prolonged heating effect on the substrate, reaching a high temperature

(1525 K), as the cooling of the substrate starts only after 14.5 µs. In contrast, the droplet impacting at 200 m/s heats the substrate to 1500 K for a short time (4.9 µs).The temperature distribution along the substrate surface at different times is shown in Fig 8d. Immediately after the droplet impact, at t=0.01 µs, the temperature rises from 450 K (initial temperature) to 1150 K, then declines abruptly to 700 K at 4.95 µm from the center as a consequence of the presence of air that has become entrapped within the droplet. This results in a modification of the heat transfer process due to the low thermal conductivity of air. At t=10.8 µs, the temperature is observed to be almost uniformly distributed across the surface.

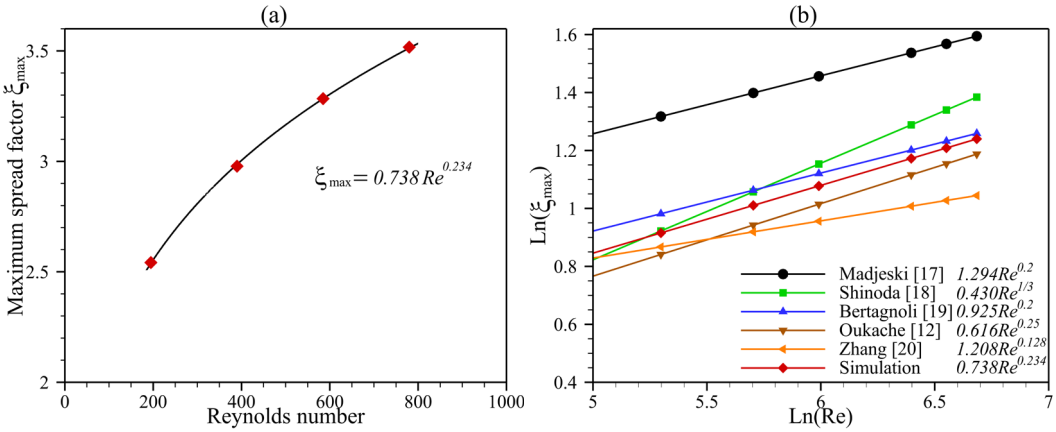

Fig. 10. Relationship between maximum spreading factor and Reynolds number (a). Comparison of different correlations (b).

Fig 9a demonstrates a significant influence of impact velocity on droplet spreading, whereby an increase in velocity results in a greater and faster spreading of the droplet. At an impact velocity of 50 m/s, the droplet reaches a maximum spreading factor of 2.5 at 2.2 µs, while at a velocity of 200 m/s; the droplet reaches maximum of 3.5 at 0.8 µs. Fig 9b illustrates an inverse relationship between splat thickness and velocity. As it increases, the droplet undergoes a greater and more rapid flattening.

Fig 10a presents the power-law interpolation equation correlating the maximum spreading factor with the Reynolds number. It is important to note that the Reynolds number ($R_e = \rho V_0 D_0 / \mu$, where ρ is the density, V_0 is the impact velocity, D_0 is the initial diameter, and μ is the droplet's viscosity) signifies the relationship between inertial forces and viscous effects. The maximum spreading factor is directly proportional to the Reynolds number, and the equation is formulated as:

$$\xi_{\max} = 0.738 R_e^{0.234} \tag{11}$$

Fig 10b shows a comparison between the correlation derived by the proposed model and others cited in the literature. Madjeski's model [17] predicts a higher spreading factor than the other models, possibly due to the theoretical approach, and solidification is considered only after the final spreading of the droplet, which is not realistic. It is very clear that the proposed relationship is very close to other correlations, especially those of Oukache [12] and Bertagnoli [19], which are based on simulation results dealing with ceramic droplets.

4. Conclusion

This paper investigates how the impact velocity of an alumina droplet influences the splat morphology, under plasma spray conditions. For this purpose, a 2D axisymmetric model based on the finite volume method has been proposed. This can simulate a multiphysics problem, including fluid dynamics, two-phase flow and heat transfer with solidification. The model was duly validated by comparing its results with published experimental data. It was observed that within the range of velocities examined, the splat takes the form of a non-splattered disk. The latter is larger and flatter at higher impact velocities, the cooling and solidification of the splat are also faster. The substrate is heated more and cools more slowly at lower velocities. According to these results, a high impact velocity is very favorable for good adhesion between the coating and the substrate, provided that this velocity is not the cause of splashed splat. A relationship between the maximum spreading factor and the Reynolds number, similar to those found in the literature, was ultimately deduced.

REFERENCES

[1] *L. Łatka, L. Pawłowski, M. Winnicki, P. Sokołowski, A. Małachowska, S. Kozerski,* Review of Functionally Graded Thermal Sprayed Coatings, Appl. Sci., Vol. 10, Iss. 15, 2020.

[2] *A. Labergue, M. Gradeck, F. Lemoine,* Comparative study of the cooling of a hot temperature surface using sprays and liquid jets, Int. J. Heat. Mass. Transf, Vol.81, 2015.

[3] *X. Liu, J. Min, X. Zhang, Z. Hu, X. Wu,* Supercooled water droplet impacting-freezing behaviors on cold superhydrophobic spheres, Int. J. Multiphase Flow, Vol. 141, 2021.

[4] *C.D. Modak, A. Kumar, A. Tripathy, P. Sen,* Drop impact printing, Nat Commun, Vol 11, 2020.

[5] *L. Pawlowski,* The Science and Engineering of Thermal Spray Coatings, 2nd edn, (John Wiley and Sons, Ltd), 2008.

[6] *K. Yang, M. Liu, K. Zhou, D. Changguang,* Recent Developments in the Research of Splat Formation Process in Thermal Spraying, Journal of Materials, 2013.

[7] *M. Bogdan, I. Peter,* A Comprehensive Understanding of Thermal Barrier Coatings (TBCs): Applications, Materials, Coating Design and Failure Mechanisms, Metals, Vol. 14, Iss. 5, 2024
[8] *K.O. Shvydyuk, J. Nunes-Pereira J, F.F. Rodrigues, A.P. Silva,* Review of Ceramic Composites in Aeronautics and Aerospace: A Multifunctional Approach for TPS, TBC and DBD Applications, Ceramics, Vol. 6, Iss. 1, 2023.
[9] *P. Fauchais, J. Heberlein; M. Boulos,* Thermal Spray Fundamentals: From Powder to Part, Springer Science & Business Media, 2014
[10] *S. Chandra and P. Fauchais,* Formation of Solid Splats During Thermal Spray Deposition, J. Thermal Spray Technol., Vol. 18, 2009.
[11] *S. Alavi, M. Passandideh-Fard, J. Mostaghimi,* Simulation of Semi-Molten Particle Impacts Including Heat Transfer and Phase Change, J Therm Spray Tech, Vol. 21, 2012.
[12] *S. Oukach, H. Hamdi, M. El Ganaoui, B. Pateyron,* Numerical study of the spreading and solidification of a molten particle impacting onto a rigid substrate under plasma spraying conditions, Thermal Science, Vol. 19, Iss. 1, 2015.
[13] *M. Shen, B.Q. Li, Q. Yang, Y. Bai, Y. Wang, S. Zhu, B. Zhao, T. Li, Y. Hu,* A modified phase-field three-dimensional model for droplet impact with solidification, International Journal of Multiphase Flow, Vol. 116, 2019.
[14] *C. Le Bot, S. Vincent, E. Meillot, F. Sarret, J. Caltagirone, L. Bianchi,* Numerical simulation of several impacting ceramic droplets with liquid/solid phase change, Surface and Coatings Technology, Vol 268, 2015.
[15] *M. Driouche, T. Rezoug, M. ohammed El Ganaoui,* Numerical study of the melting and resolidification of the substrate during the impact of a ceramic droplet in a plasma spraying process, Eur. Phys. J. Appl. Phys, Vol. 88, Iss 2, 2019.
[16] *V. Patel, A. Yadav, J. Winczek,* Computational study of the effect of spray parameters on adhesion of splat on the stainless street substrate during the impact of molten zirconia droplet, J. Heat Mass Transfer, Vol. 58, 2022.
[17] *J. Madejski,* Solidification of droplets on a cold surface, International Journal of Heat and Mass Transfer, Vol. 19, Iss 9, 1976.
[18] *K. Shinoda, T. Koseki, T. Yoshida,* Influence of impact parameters of zirconia droplets on splat formation and morphology in plasma spraying, J. Appl. Phys, Vol. 100, Iss. 7, 2006.
[19] *M. Bertagnolli, M. Marchese & G. Jacucci,* Modeling of particles impacting on a rigid substrate under plasma spraying conditions, JTST, Vol. 4, 1995.
[20] *Y. Zhang, S. Matthews, M. Hyland,* Modelling the spreading behaviour of plasma-sprayed nickel droplets under different impact conditions, J. Phys. D: Appl. Phys, Vol. 50, 2017.
[21] ANSYS FLUENT. 16.0, Theory guide, ANSYS, Inc. (2016).
[22] *J.U Brackbill, D.B Kothe, C Zemach,* A continuum method for modeling surface tension, J. Comput. Phys, Vol. 100, Iss 2, 1992.
[23] *V.R. Voller, C. Prakash,* A fixed grid numerical modelling methodology for convection-diffusion mushy region phase-change problems, Int. J. Heat. Mass. Transfer, Vol. 30, Iss 8, 1987.
[24] *Y.Z. Zheng, Q. Li, Z.H. Zheng, J.F. Zhu, P.L. Cao,* Modeling the impact, flattening and solidification of a molten dropleton a solid substrate during plasma spraying, Applied Surface Science, Vol. 317, 2014.

[25] *S.D. Aziz, S. Chandra,* Impact, Recoil and Splashing of Molten Metal Droplets, Int. J. Heat Mass Transfer, Vol. 43, Iss 16, 2000.
[26] *C. Li, J. Li,* Transient contact pressure during flattening of thermal spray droplet and its effect on splat formation, J. Therm. Spray Techno, Vol. 13, 2004.